

# Optimal 3D phase-shifting masks in partially coherent illumination

Xu Ma,<sup>1,\*</sup> Gonzalo R. Arce,<sup>2</sup> and Yanqiu Li<sup>3</sup>

<sup>1</sup>Key Laboratory of Photoelectronic Imaging Technology and System of Ministry of Education of China, School of Optoelectronics, Beijing Institute of Technology, Beijing 100081, China

<sup>2</sup>Department of Electrical and Computer Engineering, University of Delaware, Newark, Delaware 19716, USA

<sup>3</sup>Key Laboratory of Photoelectronic Imaging Technology and System of Ministry of Education of China, School of Optoelectronics, Beijing Institute of Technology, Beijing 100081, China

\*Corresponding author: maxu@bit.edu.cn

Received 12 May 2011; revised 28 June 2011; accepted 12 July 2011;  
posted 14 July 2011 (Doc. ID 147463); published 30 September 2011

Gradient-based phase-shifting mask (PSM) optimization methods have emerged as an important tool in computational lithography to solve for the inverse lithography problem under the thin-mask assumption, where the mask is considered a thin two-dimensional object. As the critical dimension printed on the wafer shrinks into the subwavelength regime, thick-mask effects become prevalent and thus these effects must be taken into account in PSM optimization methods. Thick-mask effects are particularly aggravated and pronounced in etching profiles with abrupt discontinuities and trench depths. PSM methods derived under the thin-mask assumption have inherent limitations and perform poorly in the subwavelength scenario. This paper focuses on developing three-dimensional PSM optimization methods that can overcome the thick-mask effects in lithography systems with partially coherent illumination. The boundary layer model is exploited to simplify and characterize the thick-mask effects, leading to a gradient-based PSM optimization method. Several illustrative simulations are presented. © 2011 Optical Society of America

*OCIS codes:* 110.5220, 110.4980, 050.5080, 100.3190.

## 1. Introduction

Because of the resolution limits of optical lithographic systems, the electronics industry has relied on resolution enhancement techniques (RETs) to compensate for and minimize mask distortions as they are projected onto semiconductor wafers [1,2]. Resolution in optical lithography obeys the Rayleigh resolution limit  $R = k \frac{\lambda}{NA}$ , where  $\lambda$  is the wavelength,  $NA$  is the numerical aperture, and  $k$  is the process constant, which can be minimized through RET methods [3–6]. Phase-shifting mask (PSM) methods, commonly attributed to Levenson [7], induce phase shifts in the transmitted field that have a favorable constructive or destructive interference effect. Thus,

a suitable modulation of both the intensity and the phase of the incident light can be used to effectively compensate for some of the resolution-limiting phenomena in optical diffraction.

Several approaches to PSM for inverse lithography have been proposed in the literature [8–13]. All of the algorithms above, however, have been developed under the thin-mask assumption, where Kirchhoff's boundary condition is directly applied to the mask topology and consequently the mask is treated as a two dimensional (2D) object [14,15]. As the critical dimension printed on the wafer shrinks into the subwavelength regime, the thick-mask effects become very pronounced, such that these effects should be taken into account in the mask optimization. In addition, alternating PSM employs etching profiles with abrupt discontinuities and trench depths also in the order of the wavelength [16]. This

three-dimensional (3D) topography of PSM aggravates the influence of the thick-mask effects. In this case, rigorous resource-consuming 3D simulations will be needed to evaluate the virtual electromagnetic field exiting from the mask surface. Thick-mask effects include polarization dependence due to the different boundary conditions for the electric and magnetic fields, transmission error in small openings, diffraction edge effects or electromagnetic coupling, and so on [14]. The thick-mask effects can be rigorously represented by the near field pattern of the mask, which is different from the Kirchhoff approximation of the mask topography. Two decades ago, Wong and Neureuther discovered the intensity imbalance of alternating PSM, and applied the finite-difference time-domain method (FDTD) to study the mask topography effects in the projection printing of PSM [17,18]. This phenomenon was proved by experimental results later [19]. Yuan exploited the waveguide method (WG) to model the light diffraction of two-dimensional (2D) phase-shifting masks [20], which was subsequently generalized by Lucas to the 3D topography [21]. Erdmann *et al.* evaluated and compared the FDTD method and the WG method for the simulation of a typical hyper NA ( $NA > 1$ ) imaging problem [22]. Adam and Neureuther introduced domain decomposition methods for the simulation of photomask scattering [23]. Nevertheless, these approaches are too complex to be applied in gradient-based PSM optimization.

Recently, Tirapu-Azpiroz *et al.* introduced a boundary layer (BL) model for fast evaluation of the near field of a thick mask [14,15]. Different from other computationally complex and resource-consuming rigorous mask models, the BL model effectively compensates for the inaccuracy of Kirchhoff's approximation by the complex transmission coefficients on the boundary of the mask openings. The simplicity and accuracy of the BL model enables the formulation of a gradient-based optimization algorithm for inverse lithography. Ma and Arce developed a gradient-based optical proximity correction (OPC) optimization algorithm based on the BL model to take into account the thick-mask effects in coherent imaging system [24]. However, there are three limitations to this prior work. First, the prior algorithm cannot be used directly for the PSM optimization without further extension. On the other hand, compared with OPC, PSM provides numerous advantages, but it also leads to more pronounced thick-mask effects. Thus, it is preferable to generalize the current OPC algorithm to the PSM. Second, the prior work is only tailored for the coherent imaging system. However, most practical illumination sources have a nonzero line width and their radiation is more generally described as partially coherent, which can improve the theoretical resolution limit [25,26]. A schematic of an optical lithography system with partially coherent illuminations is illustrated in Fig. 1. The light source with a wavelength of  $\lambda$  is placed at the focal plane of the first condenser, illuminating

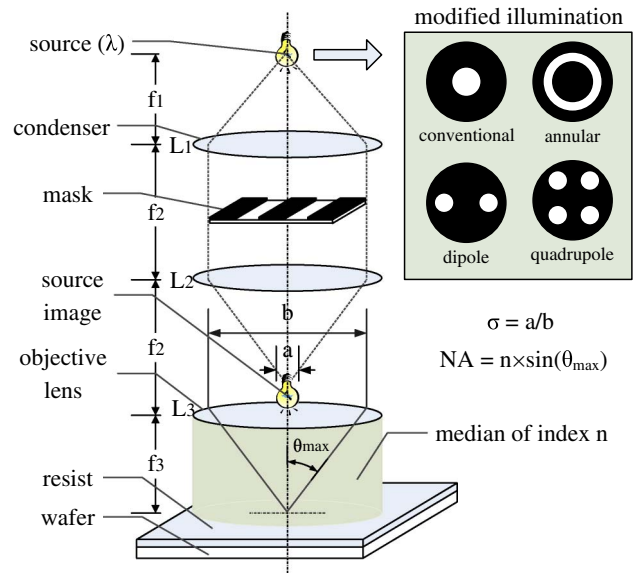


Fig. 1. (Color online) Optical lithography system with partially coherent illuminations.

the mask. Common illumination sources include dipole, quadrupole and annular shapes, all introducing partial coherence. The image of the mask is formed by the projection optics onto the wafer [1]. The partial coherence factor  $\sigma = \frac{a}{b}$  is defined as the ratio between the size of the source image on the entrance pupil (effective source) and the size of the entrance pupil.

In order to overcome these limitations above, this paper develops an efficient 3D PSM optimization algorithm in partially coherent imaging systems. This is accomplished as follows: First, the optical lithography process under partially coherent illumination is formulated as the combination of the BL model and the Fourier series expansion model. The cost function of the PSM optimization problem is formulated as the square of the  $l^2$ -norm of the difference between the real aerial image and the desired pattern on the wafer. Subsequently, the gradient of the cost function, referred to as the sensitivity of cost function, is developed and used to navigate the cost function in the descent direction during the optimization process. Topological constraints of the PSM are introduced and used to limit the minimum opening size of the optimized mask pattern. In addition, a set of methods are applied to speed up the proposed algorithm, such as the electric field caching technique (EFCT), localized topography check (LTC), and symmetrically flipping the pixels.

The remainder of the paper is organized as follows: The BL model is summarized in Section 2. The lithography preliminaries and the sensitivity of cost function are developed in Section 3. The PSM optimization algorithm based on a BL model under partially coherent illumination is described in Section 4. Simulation results are illustrated in Section 5. Conclusions are provided in Section 6.

## 2. Boundary Layer Model

### A. Boundary Layer Model in Coherent Imaging Systems

Recently, Tirapu-Azpiroz *et al.* introduced a BL model for the fast evaluation of the near field of the thick mask in coherent and partially coherent imaging systems. The details of the BL model can be found in [14–16]. In this section, we just summarize the basic concepts of the BL model. In the BL model, the near field is modeled as the superposition of the interior transmission areas and the BLs with fixed dimensions and determined locations as illustrated in Fig. 2, where the polarization of the impending electric field  $\vec{E}$  is assigned to be in the horizontal direction. Figure 2 shows a typical rectangular opening of the mask with width equal to  $a$ , and height equal to  $b$ . The near field of the opening is divided into five areas:  $A$ ,  $B$ ,  $C$ ,  $D$  and  $E$ .  $A$  is the interior transmission area with transmission coefficient  $\eta_I = 1$  or  $-1$ .  $B$  and  $D$  are the tangential boundary areas with width  $w$  and transmission coefficient  $\eta_T$ .  $C$  and  $E$  are the normal boundary areas with width  $w$  and transmission coefficient  $\eta_N$ . However, the near-field estimation obtained from the BL model is not accurate when the opening size reduces below the wavelength. For the validity of the BL model, the minimum size of the opening is constrained to be larger than the wavelength.

Tirapu-Azpiroz *et al.* studied two types of optical lithography systems. The first one is a  $4\times$  projection system with  $\text{NA} = 0.68$  and  $\lambda = 248$  nm, while the second one is with  $\text{NA} = 0.85$  and  $\lambda = 193$  nm. For both optical lithography systems, the boundary parameters of clear opening and  $180^\circ$  shifter, and the minimum opening sizes are summarized in Table 1. In the following, we will use the two types of lithography systems described by Tirapu-Azpiroz *et al.* to develop PSM optimization algorithms.

### B. Boundary Layer Model in Partially Coherent Imaging Systems

Compared with coherent illumination having a deterministic polarization, the partially coherent illumination consists of an unpolarized source. For the unpolarized source, the field polarization varies randomly, and the field components generated by different source points are not correlated and are added incoherently [16]. The BL model of partially coherent illumination is approximated as the superposition of the BL model in coherent imaging system contributed by each source point. For each source point, the BL model consists of TE and TM components. For the on-axis source point, the BL model parameters

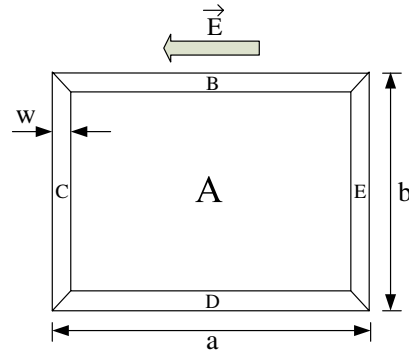


Fig. 2. (Color online) BL model under coherent illumination, where the polarization of the electric field is assigned to be in the horizontal direction,  $w$  is the width of the boundary areas, and  $a$  and  $b$  are the width and height of the entire opening area respectively.

are described in Section 2.A. For the off-axis source point, the BL parameters in Table 1 have also been proven to lead to accurate results in the  $4X$  optical lithography system with partial coherence factor  $\sigma \in [0.3, 0.6]$  [16]. The simplicity and accuracy of the BL model is suitable for the gradient-based OPC and PSM optimization algorithms [2,24].

## 3. Lithography Preliminaries and Sensitivity of Cost Function

The approximated forward imaging process of a partially coherent imaging system is illustrated in Fig. 3. In Fig. 3, the input is the mask pattern  $M$ .  $F^{\text{TE}}$  and  $F^{\text{TM}}$  are the near fields corresponding to TE and TM modes, respectively. The imaging formation process is formulated as the Fourier series expansion model represented by the second blocks in both paths, where  $\Phi_m$  is the Fourier series coefficients. The details of the Fourier series expansion model can be found in [25,27]. The final output is the aerial image  $I$ . In the following, we generalize the definitions in [24] to the PSM optimization in partially coherent imaging system.

1. The  $M_{N \times N}$  matrix represents the mask pattern, with entry values equal to  $-1$ ,  $0$  or  $1$ . The  $N^2 \times 1$  equivalent raster scanned vector representation is denoted as  $\underline{m}$ .
2. The  $\Gamma_{N \times N}(M)$  matrix represents the interior transmission area pattern of the near field corresponding to the mask  $M$ , with entry values equal to  $-1$ ,  $0$  or  $1$ . Its vector representation is denoted as  $\underline{\gamma}$ .
3. The  $F^{\text{TE}}, F^{\text{TM}} \in \mathbb{C}^{N \times N}$  represent the near fields of TE and TM modes corresponding to the mask  $M$ , where  $\mathbb{C}$  is the complex domain. Their vector representations

Table 1. Boundary Widths, Transmission Coefficients, and Corresponding Minimum Opening Sizes of the BL Model

Opening type	Boundary Width (nm)		Tangential Boundary Coefficient		Normal Boundary Coefficient	Interior Coefficient	Minimum Opening Size (nm)	
	I	II	I	II			I	II
Clear	24.8	14.5	$0.0j$	$0.8j$	0	1	248	200
$180^\circ$ shifter	55.8	53.0	$-0.52j$	$-0.30j$	0	$-1$	300	250

are denoted as  $f^{\text{TE}}$  and  $f^{\text{TM}}$ . For the phase-shifting mask in type I of the optical lithography system, the normal BLs are opaque. The tangential BLs of clear openings have transmission coefficient of 0. The tangential BLs of  $180^\circ$  phase-shifting openings have transmission coefficients of  $-0.52j$ . The pixel size is set to be  $27.9 \text{ nm}$ . The BL width of the clear opening is approximated as  $27.9 \text{ nm} = \text{pixel size}$ . The BL width of the  $180^\circ$  phase-shifting opening is  $55.8 \text{ nm} = 2 \times \text{pixel size}$ . The minimum opening size is increased to be  $306.9 \text{ nm} = 11 \times \text{pixel size}$ . Therefore, the near field of TE mode is

$$f_{-p}^{\text{TE}} = \begin{cases} -0.52j & : (\gamma_{p-2N} = -1 \text{ and } \gamma_p = 0) \text{ or } (\gamma_{p+2N} = -1 \text{ and } \gamma_p = 0) \\ \gamma_p & : \text{otherwise} \end{cases}. \quad (1)$$

$$f_{-p}^{\text{TE}} = \begin{cases} 0.8j & : (\gamma_{p-N} = 1 \text{ and } \gamma_p = 0) \text{ or } (\gamma_{p+N} = 1 \text{ and } \gamma_p = 0) \\ -0.30j & : (\gamma_{p-4N} = -1 \text{ and } \gamma_p = 0) \text{ or } (\gamma_{p+4N} = -1 \text{ and } \gamma_p = 0). \\ \gamma_p & : \text{otherwise} \end{cases}. \quad (4)$$

Equation (1) can be rewritten as

$$f_{-p}^{\text{TE}} = \frac{0.52j}{2}(1 - \gamma_p)(1 + \gamma_p)\gamma_{p-2N}(1 - \gamma_{p-2N}) + \frac{0.52j}{2}(1 - \gamma_p)(1 + \gamma_p)\gamma_{p+2N}(1 - \gamma_{p+2N}) + \gamma_p, \quad p = 1, 2, \dots, N^2, \quad (2)$$

where  $\gamma_p = 0$ , if  $p < 1$  or  $p > N^2$ . It is obvious that Eq. (1) is equal to Eq. (2). This follows for the fact that in Eq. (2),  $f_{-p}^{\text{TE}} = -0.52j$  whenever  $\gamma_{p-2N} = -1$  and  $\gamma_p = 0$ , or  $\gamma_{p+2N} = -1$  and  $\gamma_p = 0$ . Similarly, the near field of TM mode is

$$f_{-p}^{\text{TM}} = \frac{0.52j}{2}(1 - \gamma_p)(1 + \gamma_p)\gamma_{p-2}(1 - \gamma_{p-2}) + \frac{0.52j}{2}(1 - \gamma_p)(1 + \gamma_p)\gamma_{p+2}(1 - \gamma_{p+2}) + \gamma_p, \quad p = 1, 2, \dots, N^2. \quad (3)$$

For the phase-shifting mask in type II of an optical lithography system, the normal s are opaque. The tangential BLs of clear openings have transmission

coefficient of  $0.8j$ . The tangential BLs of  $180^\circ$  phase-shifting openings have transmission coefficient of  $-0.30j$ . The pixel size is set to be  $14.5 \text{ nm}$ . The BL width of the clear opening is  $14.5 \text{ nm} = \text{pixel size}$ . The BL width of the  $180^\circ$  phase-shifting opening is approximated as  $58 \text{ nm} = 4 \times \text{pixel size}$ . The minimum opening size is increased to be  $261 \text{ nm} = 18 \times \text{pixel size}$ . Therefore, the near field of TE mode is

Eq. (4) can be rewritten as

$$f_{-p}^{\text{TE}} = \frac{0.8j}{2}(1 - \gamma_p)(1 + \gamma_p)\gamma_{p-N}(1 + \gamma_{p-N}) + \frac{0.8j}{2}(1 - \gamma_p)(1 + \gamma_p)\gamma_{p+N}(1 + \gamma_{p+N}) + \frac{0.3j}{2}(1 - \gamma_p)(1 + \gamma_p)\gamma_{p-4N}(1 - \gamma_{p-4N}) + \frac{0.3j}{2}(1 - \gamma_p)(1 + \gamma_p)\gamma_{p+4N}(1 - \gamma_{p+4N}) + \gamma_p, \quad p = 1, 2, \dots, N^2, \quad (5)$$

where  $\gamma_p = 0$ , if  $p < 1$  or  $p > N^2$ . Please note that Eq. (2) is for type I optical lithography system, while Eq. (5) is for type II optical lithography system considered in this work. Similarly, the near field of TM mode is

$$f_{-p}^{\text{TM}} = \frac{0.8j}{2}(1 - \gamma_p)(1 + \gamma_p)\gamma_{p-1}(1 + \gamma_{p-1}) + \frac{0.8j}{2}(1 - \gamma_p)(1 + \gamma_p)\gamma_{p+1}(1 + \gamma_{p+1}) + \frac{0.3j}{2}(1 - \gamma_p)(1 + \gamma_p)\gamma_{p-4}(1 - \gamma_{p-4}) + \frac{0.3j}{2}(1 - \gamma_p)(1 + \gamma_p)\gamma_{p+4}(1 - \gamma_{p+4}) + \gamma_p, \quad p = 1, 2, \dots, N^2. \quad (6)$$

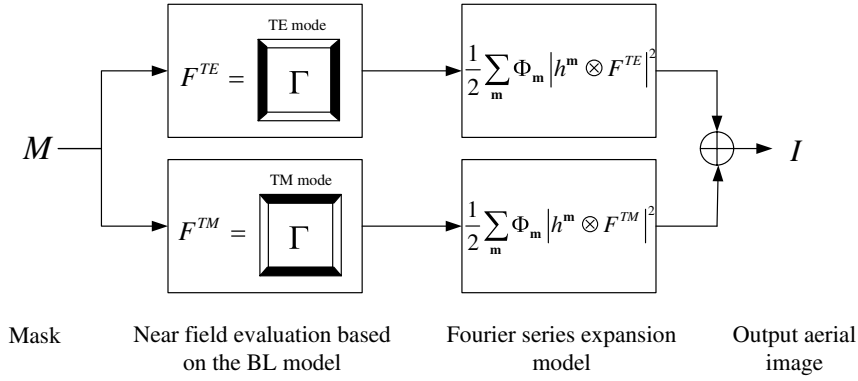


Fig. 3. Approximated forward imaging process based on the BL model under partially coherent illumination.

Please note that Eq. (3) is for the type I optical lithography system, while Eq. (6) is for the type II optical lithography system considered in this work.

4. The two-dimensional filter  $h^m$  is the amplitude impulse response of each coherent component of the overall partially coherent imaging system. Let  $\mathbf{r} = (x, y)$  represent the coordinates in both the object plane and the image plane and  $\gamma(\mathbf{r})$  be the complex degree of coherence. Assume the mask is constrained in the square area  $A$  defined by  $x, y \in [-D/2, D/2]$ . Thus, the only values of  $\gamma(\mathbf{r})$  needed are those inside the square area  $A_\gamma$  defined by  $x, y \in [-D, D]$ . Applying the 2D Fourier series expansion,  $\gamma(\mathbf{r})$  can be rewritten as

$$\gamma(\mathbf{r}) = \sum_{\mathbf{m}} \Gamma_{\mathbf{m}} \exp(j\omega_0 \mathbf{m} \cdot \mathbf{r}), \quad (7)$$

and

$$\Gamma_{\mathbf{m}} = \frac{1}{D^2} \int_{A_\gamma} \gamma(\mathbf{r}) \exp(j\omega_0 \mathbf{m} \cdot \mathbf{r}) d\mathbf{r}, \quad (8)$$

where  $\omega_0 = \pi/D$ ,  $\mathbf{m} = (m_x, m_y)$ ,  $m_x$  and  $m_y$  are integers, and  $\cdot$  is the inner-product operation. In addition, let  $h(\mathbf{r})$  be the amplitude impulse response of the optical system. Therefore,

$$h^m(\mathbf{r}) = h(\mathbf{r}) \exp(j\omega_0 \mathbf{m} \cdot \mathbf{r}). \quad (9)$$

5. The desired  $N \times N$  binary output pattern is denoted as  $\tilde{I}$ . It is the desired aerial image sought on the wafer. Its vector representation is denoted as  $\tilde{i}$ .

6.  $\bar{\Gamma}$  is the initial interior transmission area of the optimization process. The amplitude of  $\bar{\Gamma}$  is assigned equal to  $\tilde{I}$ . The phase of  $\bar{\Gamma}$  must be assigned a priori, where phases in neighboring blocks are assigned alternately. For each  $\bar{\Gamma}$ , the corresponding initial mask pattern is  $\hat{M}$ .

7. The output aerial image is the  $N \times N$  matrix denoted as

$$I = \frac{1}{2} \sum_{\mathbf{m}} \Phi_{\mathbf{m}} \|h^m \otimes F^{TE}\|^2 + \frac{1}{2} \sum_{\mathbf{m}} \Phi_{\mathbf{m}} \|h^m \otimes F^{TM}\|^2, \quad (10)$$

where  $\otimes$  is the convolution operator. The equivalent vector is denoted as  $\underline{i}$ .

8. The optimized mask denoted as  $\hat{M}$  minimizes the distance between  $I$  and  $\tilde{I}$ , ie,

$$\hat{M} = \underset{M}{\operatorname{argmin}} d(i, \tilde{i}). \quad (11)$$

The cost function is the square of the  $l^2$ -norm of the difference between  $\underline{i}$  and  $\tilde{i}$ . Therefore,

$$d = F(\underline{\gamma}) = \|\underline{i} - \tilde{i}\|_2^2 = \sum_{p=1}^{N^2} (i_p - \tilde{i}_p)^2, \quad (12)$$

where

$$i_p = \frac{1}{2} \sum_{\mathbf{m}} \Phi_{\mathbf{m}} \left| \sum_{q=1}^{N^2} h_{pq}^m f_{L_q}^{TE} \right|^2 + \frac{1}{2} \sum_{\mathbf{m}} \Phi_{\mathbf{m}} \left| \sum_{q=1}^{N^2} h_{pq}^m f_{L_q}^{TM} \right|^2, \quad (13)$$

$$p = 1, \dots, N^2,$$

where  $h_{pq}^m$  is the  $p, q$ th entry of the filter  $h^m$ .

The performance of the PSM optimization algorithm is evaluated by the output pattern error, which is defined as  $d$  in Eq. (12). In the following, the sensitivity of cost function  $F$  with respect to the change of the interior transmission area will be used to guide the optimization process. The sensitivity of cost function  $F$  is  $\nabla F$ . The sensitivities of cost function for both types of the optical lithography systems are described in Appendix A.

#### 4. 3D PSM Optimization Algorithm Based on BL Model

##### A. Topological Constraint

According to the BL model summarized in Section 2, the interior transmission area has a one-to-one correspondence to the mask. Therefore, the proposed algorithm directly optimizes the interior transmission area, from which the mask can be easily reconstructed. The BL model constrains the minimum size of the openings on PSM [14,15]. In order to meet the requirements, some topological constraints are

imposed in the optimization process of the interior transmission area. In the following, some definitions and operations for shape topologies are listed.

**Definition 1** (White, gray and black blocks). Any pixel in the interior transmission area can have a value 1, 0 or  $-1$ . A white, black, or gray block is a square area with all pixels values equal to 1,  $-1$ , or 0, respectively.

**Definition 2** (Flipping on and flipping off operations). Increasing or decreasing a pixel value by 1 is referred to as flipping on or flipping off a pixel. In general, consider a block with maximum pixel value  $p_{\max}$  and minimum pixel value  $p_{\min}$ . If  $p_{\max} = 1$ , a flipping on operation means to turn the block to a white block. Otherwise, a flipping on operation means assigning all the pixel values in this block equal to  $p_{\max} + 1$ . Similarly, if  $p_{\min} = -1$ , a flipping off operation means turning the block to a black block. Otherwise, a flipping off operation means assigning all of the pixel values in this block equal to  $p_{\min} - 1$ .

**Definition 3** (Type I and II singular pixels). A type I or II singular pixel is a white or black pixel that does not belong to any  $L_1 \times L_1$  white or black block on the interior transmission area pattern  $\Gamma$ , where  $L_1$  depends on the minimum opening size of the BL model.

**Definition 4** (Type III singular pixel). A type III singular pixel is a gray pixel that does not belong to any  $L_2 \times L_2$  gray block on the interior transmission area pattern  $\Gamma$ . Since the openings on the optimized PSM contain the additional surrounding BLs compared to the corresponding interior transmission areas, the type III singular pixel introduces the merge of adjacent openings on the mask.

**Definition 5** (Type IV singular pixel). A type IV singular pixel is a white or black pixel that is adjacent to a black or white pixel. The type IV singular pixel also introduces the merge of adjacent openings on the mask.

**Definition 6** (Cost sensitivity matrix of a block). Given a block  $G^{K \times K}$ , the cost sensitivity matrix  $\nabla F(G)^{K \times K}$ , which is supported by the location of  $G$ , and calculated by Eq. (A1) or Eq. (A2), is defined as the cost sensitivity matrix of the block  $G$ .

**Definition 7** (Cost sensitivity statistics of a block). The cost sensitivity statistics of a block  $G$  is  $S(G) = \text{sum}\{|\nabla F(G)|\}$ , where  $\text{sum}\{\}$  means the summation of all entries of the matrix in the argument. The block with larger cost sensitivity statistics has higher priority to be flipped.

**Definition 8** (Changeable block). A  $K \times K$  changeable block is a block whose cost sensitivity matrix contains  $K$  positive or negative values. If the cost sensitivity matrix contains  $K$  positive values, the block is defined as a positive changeable block. Vice versa, it is defined as a negative changeable block. Note that a block may be both positive and negative changeable blocks at the same time.

In our PSM optimization approach, only the positive or negative changeable blocks are considered to be flipped off or flipped on. These topological

constraints guarantee that the features of the optimized PSM are larger than the minimum opening size.

## B. 3D PSM Optimization Algorithm

Following the topological constraints, the proposed PSM optimization algorithm is summarized in the following:

**Step 1:** Initialization of the amplitude of interior transmission area pattern:  $|\bar{\Gamma}| = I$ . The phase of  $\bar{\Gamma}$  must be assigned a priori, where phases in neighboring blocks are assigned alternately. The corresponding initial mask pattern is  $\bar{M}$ .

**Step 2:** Calculate the cost sensitivity function using Eq. (A1) for type I optical lithography system or Eq. (A2) for type II optical lithography system.

**Step 3:** Find a  $K \times K$  block  $G$ , which has not been transversed and has the largest cost sensitivity statistics. Then, check if  $G$  is a changeable block.

If  $G$  is a changeable block, go to step 4.

Otherwise, mark  $G$  to be transversal, and repeat step 3.

**Step 4:** Flip on or flip off  $G$  if it is a negative or positive changeable block.

**Step 5:** If the cost function  $F$  is increased flag = 1.

**Step 6:** If (flag == 1) or (flipping operation has introduced type I-IV singular pixels), restore  $G$  to its original values.

**Step 7:** If any block  $G$  has not been transversed in step 3, go to step 3.

Otherwise, if no block is flipped in the current iteration, end.

Otherwise go to step 2.

In the proposed algorithm, the parameters  $K$  in **Step 3** and  $L_1$  used in *Definition 3* depend on the minimum opening size assigned in Section 2.A, and their values will be described shortly in Section 5. In *Definition 4*,  $L_2 = 5$  and 9 for type I and type II optical lithography systems, respectively.

## C. Algorithm Acceleration

In this section, we describe a set of methods to speed up the proposed algorithm. In the proposed algorithm, whenever any block is flipped, we need to recalculate the aerial image and check whether the cost function is increased. It is known that the aerial image calculation is computational complex. In order to reduce the computational intensity of the proposed algorithm, the EFCT is applied to speed up the aerial image calculation [28,29]. In the following, we just discuss the EFCT for the TE mode, and the case for the TM mode is similar. Initially, we calculate and save every electric field component  $E^{\text{TE}m}$  in the partially coherent system. According to Eq. (10), we have

$$E^{\text{TE}m}(x,y) = F^{\text{TE}}(x,y) \otimes h^m(x,y). \quad (14)$$

During the block flip operation, if  $F^{\text{TE}}(x_0,y_0)$  is modified to  $F^{\text{TE}'}(x_0,y_0)$ , the electric field component is updated as

$$E^{\text{TE}m'}(x,y) = E^{\text{TE}m}(x,y) + [F^{\text{TE}'}(x_0,y_0) - F^{\text{TE}}(x_0,y_0)] \times h^m(x-x_0,y-y_0). \quad (15)$$

Whenever the electric field components are updated, the aerial image can be calculated by

$$I(x,y) = \frac{1}{2} \sum_m \Phi_m |E^{\text{TE}m}(x,y)|^2 + \frac{1}{2} \sum_m \Phi_m |E^{\text{TM}m}(x,y)|^2. \quad (16)$$

Each time a  $K \times K$  block is flipped, the EFCT is only applied to a small area on the near field supported by the flipped block. Therefore, the computational intensity incurred by the aerial image calculation is effectively alleviated. However, one disadvantage of the EFCT is that the aerial images calculated by EFCT and Eq. (10) are not perfectly equal to each other. Although the difference is very small, error accumulation will become pronounced after a number of iterations. In order to solve this problem, we reset the electric fields using Eq. (14) whenever we applied EFCT for 10 times.

Another method to speed up the proposed algorithm is through the use of the LTC method. In **Step 6** of the proposed algorithm, we need to check whether the flip operation introduces type I-IV singular pixels. Since each time we only flip a  $K \times K$  block  $G$ , we exploit the LTC method, which means we only check the local topography that is influenced by  $G$ .

Finally, if the desired pattern is symmetric with respect to some axis, then the optimization process is carried out just in one half of the mask. The sym-

metric pixels with respect to this axis on the other side are flipped in the same way. This algorithm acceleration method is referred to as the symmetric operation (SO). In order to illustrate the effectiveness of the above algorithm acceleration approaches, the runtime reduction due to different algorithm acceleration methods is provided in Section 5.

## 5. Simulations

To prove the effectiveness of the proposed PSM optimization algorithm, the method described in Section 4.B is used to design a mask targeting a desired pattern of two vertical bars. We also compare the PSMs optimized using the proposed algorithm and the thin-mask optimization method. For type I optical lithography system, the simulation results are shown in Fig. 4, where  $\text{NA} = 0.68$ ,  $\lambda = 248 \text{ nm}$ , and  $K = L_1 = 9$ . The illumination is an annular illumination with  $\sigma_{\text{inner}} = 0.3$  and  $\sigma_{\text{outer}} = 0.4$ . Since the system is a 4X projection system, the convolution kernel is scaled as

$$h(\mathbf{r}) = \frac{J_1(2\pi r \text{NA}'/\lambda)}{2\pi r \text{NA}'/\lambda}, \quad (17)$$

where  $\text{NA}' = \frac{1}{4} \text{NA}$ . The convolution kernel is assumed to vanish outside the area  $A_{h1}$  defined by  $x, y \in [-279 \text{ nm}, 279 \text{ nm}]$ . Figure 4(a) is the initial mask, and Fig. 4(d) is the corresponding aerial image with pattern error of 557.6. Figure 4(b) is the optimized PSM using the algorithm depicted in Section 4.B based on thin-mask approximation, and Fig. 4(e) is the corresponding aerial image with

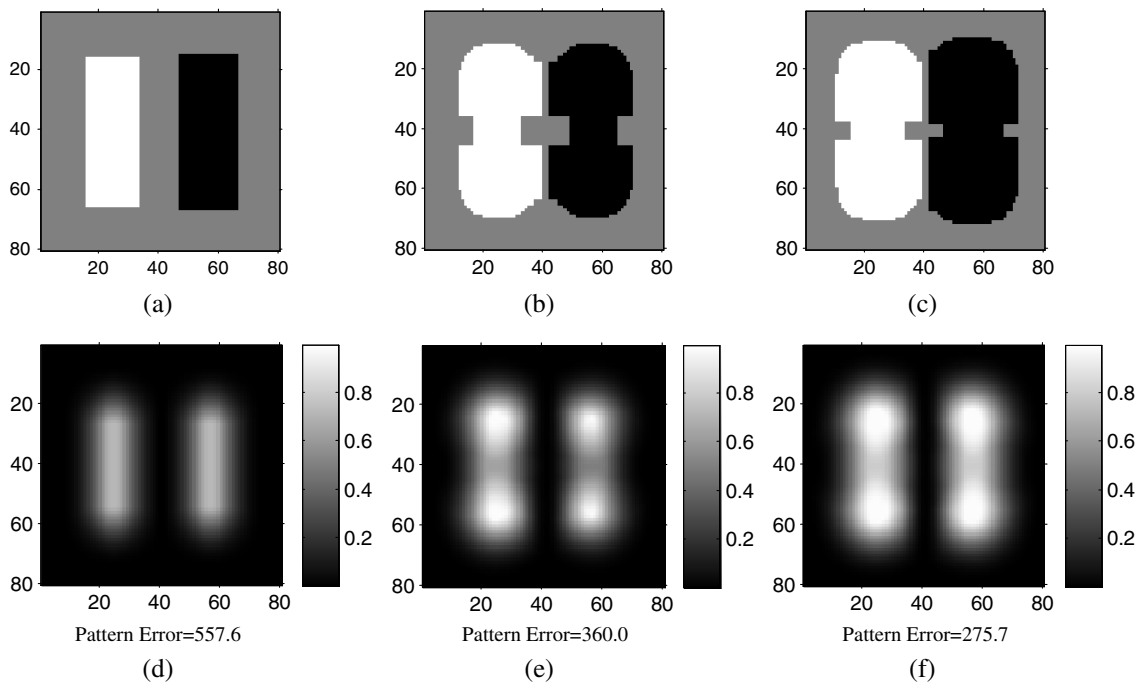


Fig. 4. PSM optimization for type I optical lithography system.  $\text{NA} = 0.68$  and  $\lambda = 248 \text{ nm}$ . (a) the initial mask; (b) the optimized PSM based on thin-mask approximation; (c) the optimized PSM based on BL model. (d), (e) and (f) show the aerial images corresponding to (a), (b) and (c), respectively. In the mask patterns, black, gray and white represent  $-1$ ,  $0$  and  $1$ , respectively.

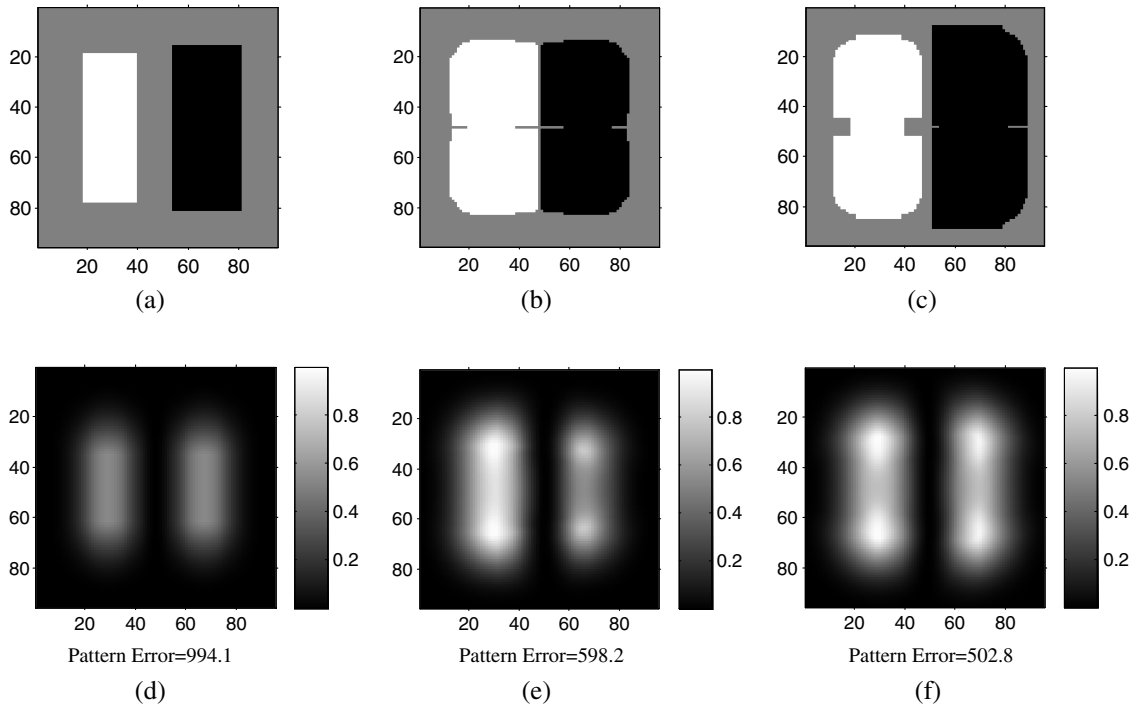


Fig. 5. PSM optimization for type II optical lithography system.  $NA = 0.85$  and  $\lambda = 193$  nm. (a) the initial mask; (b) the optimized PSM based on thin-mask approximation; (c) the optimized PSM based on BL model. (d), (e) and (f) show the aerial images corresponding to (a), (b) and (c), respectively. In the mask patterns, black, gray and white represent  $-1$ ,  $0$  and  $1$ , respectively.

pattern error of 360. Figure 4(c) is the optimized 3D PSM using the proposed algorithm based on the BL model, and Fig. 4(f) is the corresponding aerial image with pattern error of 275.7. In the mask patterns, black, gray, and white represent  $-1$ ,  $0$  and  $1$ , respectively. It is shown that optimization of the PSM based on thin-mask approximation reduces the pattern error by 35%. On the other hand, the proposed 3D PSM optimization algorithm reduces the pattern error by 51%. It is also noted that the thin-mask approximation leads to the intensity imbalance between the aerial images exposed by the clear opening and  $180^\circ$  shifter. On the other hand, the intensity imbalance is alleviated by the proposed algorithm. In order to prove the effectiveness of the algorithm acceleration approaches described in Section 4.C, the runtime based on different algorithm acceleration methods is summarized in Table 2. The runtime of the proposed algorithm without any algorithm acceleration approach is 6691 s. The runtime of the proposed algorithm with EFCT is 1645 s. The runtime of the proposed algorithm with EFCT and LTC is 1462 s. The runtime of the proposed algorithm with EFCT, LTC, and SO is 315 s. It is clear that the proposed algorithm acceleration approaches can effectively improve the computational efficiency of the optimization algorithm.

For type II optical lithography system, the simulation results are shown in Fig. 5, where  $NA = 0.85$ ,  $\lambda = 193$  nm and  $K = L_1 = 16$ . The illumination is an annular illumination with  $\sigma_{\text{inner}} = 0.3$  and  $\sigma_{\text{outer}} = 0.4$ . The convolution kernel is assumed to vanish outside the area  $A_{h2}$  defined by  $x, y \in [-217.5 \text{ nm}, 217.5 \text{ nm}]$ . In Fig. 5, the initial mask leads to a pattern error of 994.1. The PSM optimized based on thin-mask approximation leads to a pattern error of 598.2. The optimized 3D PSM using the proposed algorithm based on a BL model leads to a pattern error of 502.8. It is shown that optimization of the PSM based on thin-mask approximation reduces the pattern error by 40%. On the other hand, the proposed 3D PSM optimization algorithm reduces the pattern error by 49%. It is also noted that the thin-mask approximation leads to the intensity imbalance between the aerial images exposed by the clear opening and  $180^\circ$  shifter. On the other hand, the intensity imbalance is alleviated by the proposed algorithm. The runtime reduction due to different algorithm acceleration approaches is summarized in Table 2.

The performance differences between optimizing mask based on the thin-mask approximation and the BL model show the necessity of the proposed algorithms to take into account the thick-mask effects. It should be noted that other factors such as the

Table 2. Runtime Reduction Because of Different Algorithm Acceleration Approaches

Lithography System Types	Without Algorithm Acceleration (s)	EFCT (s)	EFCT +LTC(s)	EFCT +LTC +SO(s)
Type I	6691	1645	1462	315
Type II	10904	1774	1679	1076

radiometric factor should be taken into account for the optical lithography system with  $NA$  larger than 0.6. The radiometric factor shows that for a projection reduction lithography system, the amplitude of higher spatial frequency component of the diffractive light is amplified. Such considerations fall outside the scope of our paper and are topics for future work.

## 6. Conclusion

This paper studies the gradient-based PSM optimization algorithm taking into account the thick-mask effects under partially coherent imaging systems.

The BL model is applied to evaluate the near field of the thick mask. Based on this model, the PSM optimization algorithm is proposed for two typical kinds of lithography systems. Topological constraints are applied in the optimization framework to limit the minimum feature size on the mask. Simulations illustrate that the proposed approach is effective and practical.

## Appendix A

For type I optical lithography system, the sensitivity of cost function can be calculated as

$$\begin{aligned}
\nabla F = & -2\text{Re} \left\{ \sum_{\mathbf{m}} \Phi_{\mathbf{m}} \{ h^{\mathbf{m}*} \otimes [(\tilde{I} - I) \odot (h^{\mathbf{m}} \otimes F^{\text{TE}})] \odot [0.52j\Gamma \odot \Gamma \uparrow_2 \odot (1 - \Gamma \uparrow_2) + 0.52j\Gamma \odot \Gamma \downarrow_2 \odot (1 - \Gamma \downarrow_2) + 1] \right. \\
& + \{ h^{\mathbf{m}*} \otimes [(\tilde{I} - I) \odot (h^{\mathbf{m}} \otimes F^{\text{TE}})] \} \uparrow_2 \odot [-0.26j(1 - \Gamma \uparrow_2) \odot (1 + \Gamma \uparrow_2) \odot (1 - 2\Gamma)] \\
& + \{ h^{\mathbf{m}*} \otimes [(\tilde{I} - I) \odot (h^{\mathbf{m}} \otimes F^{\text{TE}})] \} \downarrow_2 \odot [-0.26j(1 - \Gamma \downarrow_2) \odot (1 + \Gamma \downarrow_2) \odot (1 - 2\Gamma)] \} \\
& + \sum_{\mathbf{m}} \Phi_{\mathbf{m}} \{ h^{\mathbf{m}*} \otimes [(\tilde{I} - I) \odot (h^{\mathbf{m}} \otimes F^{\text{TM}})] \odot [0.52j\Gamma \odot \Gamma \leftarrow_2 \odot (1 - \Gamma \leftarrow_2) + 0.52j\Gamma \odot \vec{\Gamma}_2 \odot (1 - \vec{\Gamma}_2) + 1] \right. \\
& + \{ h^{\mathbf{m}*} \otimes [(\tilde{I} - I) \odot (h^{\mathbf{m}} \otimes F^{\text{TM}})] \} \leftarrow_2 \odot [-0.26j(1 - \Gamma \leftarrow_2) \odot (1 + \Gamma \leftarrow_2) \odot (1 - 2\Gamma)] \\
& + \overrightarrow{\{ h^{\mathbf{m}*} \otimes [(\tilde{I} - I) \odot (h^{\mathbf{m}} \otimes F^{\text{TM}})] \} \leftarrow_2} \odot [-0.26j(1 - \vec{\Gamma}_2) \odot (1 + \vec{\Gamma}_2) \odot (1 - 2\Gamma)] \} \}, \tag{A1}
\end{aligned}$$

where  $\odot$  is the element-by-element multiplication operator.  $h^\circ$  rotates  $h$  by  $180^\circ$ . The notation  $*$  represents complex conjugate.  $\{\} \uparrow_n$ ,  $\{\} \downarrow_n$ ,  $\{\} \leftarrow_n$  and  $\{\} \rightarrow_n$  are shifting operations by shifting the  $N \times N$

matrix in the argument along the arrow directions (up, down, left, and right) by  $n$  pixels, respectively. For type II optical lithography system, the sensitivity of cost function can be calculated as

$$\begin{aligned}
\nabla F = & -2\text{Re} \sum_{\mathbf{m}} \Phi_{\mathbf{m}} \{ h^{\mathbf{m}*} \otimes [(\tilde{I} - I) \odot (h^{\mathbf{m}} \otimes F^{\text{TE}})] \odot [0.3j\Gamma \odot \Gamma \uparrow_4 \odot (1 - \Gamma \uparrow_4) + 0.3j\Gamma \odot \Gamma \downarrow_4 \odot (1 - \Gamma \downarrow_4) \\
& + 0.8j\Gamma \odot \Gamma \uparrow \odot (1 - \Gamma \uparrow) + 0.8j\Gamma \odot \Gamma \downarrow \odot (1 - \Gamma \downarrow) + 1] \\
& + \{ h^{\mathbf{m}*} \otimes [(\tilde{I} - I) \odot (h^{\mathbf{m}} \otimes F^{\text{TE}})] \} \uparrow \odot [-0.4j(1 - \Gamma \uparrow) \odot (1 + \Gamma \uparrow) \odot (1 + 2\Gamma)] \\
& + \{ h^{\mathbf{m}*} \otimes [(\tilde{I} - I) \odot (h^{\mathbf{m}} \otimes F^{\text{TE}})] \} \downarrow \odot [-0.4j(1 - \Gamma \downarrow) \odot (1 + \Gamma \downarrow) \odot (1 + 2\Gamma)] \\
& + \{ h^{\mathbf{m}*} \otimes [(\tilde{I} - I) \odot (h^{\mathbf{m}} \otimes F^{\text{TE}})] \} \uparrow_4 \odot [-0.15j(1 - \Gamma \uparrow_4) \odot (1 + \Gamma \uparrow_4) \odot (1 - 2\Gamma)] \\
& + \{ h^{\mathbf{m}*} \otimes [(\tilde{I} - I) \odot (h^{\mathbf{m}} \otimes F^{\text{TE}})] \} \downarrow_4 \odot [-0.15j(1 - \Gamma \downarrow_4) \odot (1 + \Gamma \downarrow_4) \odot (1 - 2\Gamma)] \} \\
& + \sum_{\mathbf{m}} \Phi_{\mathbf{m}} \{ h^{\mathbf{m}*} \otimes [(\tilde{I} - I) \odot (h^{\mathbf{m}} \otimes F^{\text{TM}})] \odot [0.3j\Gamma \odot \Gamma \leftarrow_4 \odot (1 - \Gamma \leftarrow_4) + 0.3j\Gamma \odot \vec{\Gamma}_4 \odot (1 - \vec{\Gamma}_4) \\
& + 0.8j\Gamma \odot \Gamma \leftarrow \odot (1 - \Gamma \leftarrow) + 0.8j\Gamma \odot \vec{\Gamma} \odot (1 - \vec{\Gamma}) + 1] \\
& + \{ h^{\mathbf{m}*} \otimes [(\tilde{I} - I) \odot (h^{\mathbf{m}} \otimes F^{\text{TM}})] \} \leftarrow \odot [-0.4j(1 - \Gamma \leftarrow) \odot (1 + \Gamma \leftarrow) \odot (1 + 2\Gamma)] \\
& + \overrightarrow{\{ h^{\mathbf{m}*} \otimes [(\tilde{I} - I) \odot (h^{\mathbf{m}} \otimes F^{\text{TM}})] \} \leftarrow} \odot [-0.4j(1 - \vec{\Gamma}) \odot (1 + \vec{\Gamma}) \odot (1 + 2\Gamma)] \\
& + \{ h^{\mathbf{m}*} \otimes [(\tilde{I} - I) \odot (h^{\mathbf{m}} \otimes F^{\text{TM}})] \} \leftarrow_4 \odot [-0.15j(1 - \Gamma \leftarrow_4) \odot (1 + \Gamma \leftarrow_4) \odot (1 - 2\Gamma)] \\
& + \overrightarrow{\{ h^{\mathbf{m}*} \otimes [(\tilde{I} - I) \odot (h^{\mathbf{m}} \otimes F^{\text{TM}})] \} \leftarrow_4} \odot [-0.15j(1 - \vec{\Gamma}_4) \odot (1 + \vec{\Gamma}_4) \odot (1 - 2\Gamma)] \} \}. \tag{A2}
\end{aligned}$$

We are grateful for financial support by the Key Program of the National Natural Science Foundation of China (NSFC) under No. 60938003, the National Science and Technology Major Project, the Program of Education Ministry for Changjiang Scholars in University, the Excellent Young Scholars Research Foundation of Beijing Institute of Technology (Grant No. 2010Y0408), and the Basic Research Foundation of Beijing Institute of Technology. Our work is also supported by the Program for New Century Excellent Talents in University.

## References

1. A. K. Wong, *Resolution Enhancement Techniques*, Vol. 1 (SPIE, 2001).
2. X. Ma and G. R. Arce, *Computational Lithography*, 1st ed., Wiley Series in Pure and Applied Optics (Wiley, 2010).
3. S. A. Campbell, *The Science and Engineering of Microelectronic Fabrication*, 2nd ed. (Publishing House of Electronics Industry, 2003).
4. F. Schellenberg, "Resolution enhancement technology: The past, the present, and extensions for the future, optical microlithography," *Proc. SPIE* **5377**, 1–20 (2004).
5. F. Schellenberg, *Resolution Enhancement Techniques in Optical Lithography* (SPIE, 2004).
6. L. Liebmann, S. Mansfield, A. Wong, M. Lavin, W. Leipold, and T. Dunham, "Tcad development for lithography resolution enhancement," *IBM J. Res. Dev.* **45**, 651–665 (2001).
7. M. D. Levenson, N. S. Viswanathan, and R. A. Simpson, "Improving resolution in photolithography with a phase-shifting mask," *IEEE Trans. Electron Devices* **29**, 1828–1836 (1982).
8. Y. Liu and A. Zakhor, "Binary and phase shifting mask design for optical lithography," *IEEE Trans. Semicond. Manuf.* **5**, 138–152 (1992).
9. Y. C. Pati and T. Kailath, "Phase-shifting masks for microlithography: Automated design and mask requirements," *J. Opt. Soc. Am. A* **11**, 2438–2452 (1994).
10. A. Poonawala and P. Milanfar, "Opc and psm design using inverse lithography: A non-linear optimization approach," *Proc. SPIE* **6154**, 1159–1172 (2006).
11. X. Ma and G. R. Arce, "Generalized inverse lithography methods for phase-shifting mask design," *Opt. Express* **15**, 15066–15079 (2007).
12. X. Ma and G. R. Arce, "Psm design for inverse lithography with partially coherent illumination," *Opt. Express* **16**, 20126–20141 (2008).
13. X. Ma and G. R. Arce, "Pixel-based simultaneous source and mask optimization for resolution enhancement in optical lithography," *Opt. Express* **17**, 5783–5793 (2009).
14. J. Tirapu-Azpiroz, P. Burchard, and E. Yablonovitch, "Boundary layer model to account for thick mask effects in photolithography," *Proc. SPIE* **5040**, 1611–1619 (2003).
15. J. Tirapu-Azpiroz and E. Yablonovitch, "Fast evaluation of photomask near-fields in sub-wavelength 193 nm lithography," *Proc. SPIE* **5377**, 1528–1535 (2004).
16. J. Tirapu-Azpiroz, "Analysis and modeling of photomask near-fields in sub-wavelength deep ultraviolet lithography with optical proximity corrections," Ph.D. thesis (University of California–Los Angeles, 2004).
17. A. Wong, "Rigorous three-dimensional time-domain finite difference electromagnetic simulation," Ph.D. thesis (University of California–Berkeley, 1994).
18. A. Wong and A. R. Neureuther, "Mask topography effects in projection printing of phase shift masks," *IEEE Trans. Electron Devices* **41**, 895–902 (1994).
19. C. Pierrat, A. Wong, and S. Vaidya, "Phase-shifting mask topography effects on lithographic image quality," in *International Electron Devices Meeting (IEDM '92)*, Technical Digest (1992), pp. 53–56.
20. C. M. Yuan, "Calculation of one-dimension lithographic aerial images using the vector theory," *IEEE Trans. Electron Devices* **40**, 1604–1613 (1993).
21. K. Lucas, H. Tanabe, and A. J. Strojwas, "Efficient and rigorous three-dimensional model for optical lithography simulation," *J. Opt. Soc. Am. A* **13**, 2187–2199 (1996).
22. A. Erdmann, P. Evanschitzky, G. Citarella, T. Fühner, and P. D. Bisschop, "Rigorous mask modeling using waveguide and fldtd methods: An assessment for typical hyper na imaging problems," *Proc. SPIE* **6283**, 628319 (2006).
23. K. Adam and A. R. Neureuther, "Domain decomposition methods for the rapid electromagnetic simulation of photomask scattering," *J. Microlithogr. Microfabrication Microsyst.* **1**, 253–269 (2002).
24. X. Ma and G. R. Arce, "Binary mask optimization for forward lithography based on boundary layer model in coherent systems," *J. Opt. Soc. Am. A* **26**, 1687–1695 (2009).
25. X. Ma and G. R. Arce, "Binary mask optimization for inverse lithography with partially coherent illumination," *J. Opt. Soc. Am. A* **25**, 2960–2970 (2008).
26. X. Ma and G. R. Arce, "Pixel-based opc optimization based on conjugate gradients," *Opt. Express* **19**, 2165–2180 (2011).
27. B. E. A. Saleh and M. Rabbani, "Simulation of partially coherent imagery in the space and frequency domains and by modal expansion," *Appl. Opt.* **21**, 2770–2777 (1982).
28. Y. Granik, "Solving inverse problem of optical microlithography," *Proc. SPIE* **5754**, 506–526 (2004).
29. X. Ma and Y. Li, "Resolution enhancement optimization methods in optical lithography with improved manufacturability," *J. Micro/Nanolith. MEMS MOEMS* **10**, 023009 (2011).